THE JOURNAL OF PHYSICAL CHEMISTRY A

pubs.acs.org/JPCA Article

Three-Photon Spectroscopy of Porphyrins

Luca Ravotto, Stephen L. Meloni, Tatiana V. Esipova, Artëm E. Masunov, Jessica M. Anna, and Sergei A. Vinogradov*

Cite This: *J. Phys. Chem. A* 2020, 124, 11038−11050 Read Online

ACCESS | Metrics & More | Article Recommendations | Supporting Information

ABSTRACT: Recent advances in laser technology have made three-photon (3P) microscopy a real possibility, raising interest in the phenomenon of 3P absorption (3PA). Understanding 3PA of organic chromophores is especially important in view of those imaging applications that rely on exogenous probes, whose optical properties can be manipulated and optimized. Here, we present measurements and theoretical analysis of the degenerate 3PA spectra of several phosphorescent metalloporphyrins, which are used in the construction of biological oxygen probes. The effective 3PA cross sections ($\sigma^{(3)}$) of these porphyrins near 1700 nm, a new promising biological optical window, were found to be on the order of 1000 GM3 (1 GM3 = 10^{-83} cm^6 s^2), therefore being among the highest values reported to date for organic chromophores. To interpret our data, we developed a qualitative four-state model specific for porphyrins and used it in conjunction with quantitative analysis based on the time-dependent density functional theory (TDDFT)/*a posteriori* Tamm−Dancoff approximation (ATDA)/sum-over-states (SOS) formalism. The analysis revealed that B (Soret) state plays a key role in the enhancement of 3PA of porphyrins in the Q band region, while the low-lying two-photon (2P)-allowed gerade states interfere negatively and diminish the 3PA strength. This study features the first systematic examination of 3PA properties of porphyrins, suggesting ways to improve their performance and optimize them for imaging and other biomedical applications.

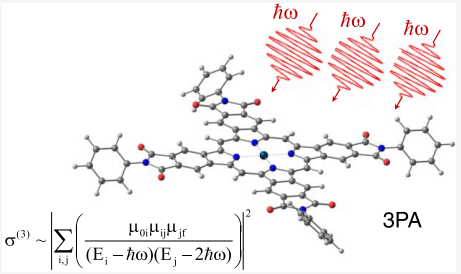

INTRODUCTION

Following its invention in the early 1990s, two-photon (2P) microscopy has become one of the most popular tools for deep-tissue imaging, owing to its unique ability to probe biological processes in intact tissues at depth with high spatial resolution.[1] The key advantage of 2P excitation is its ability to confine absorption of light to the immediate vicinity of the laser focus while shifting the excitation energy to the near-infrared region of the spectrum. Excitation at longer wavelengths results in less scattering, less absorption by endogenous chromophores, and consequently lesser risk of photodamage. At the same time, near-focal confinement makes 2P microscopy especially valuable for maintaining depth-resolution in scattering media, such as in the rodent brain cortex, where important physiological processes can be observed and quantified already several hundred microns below the tissue surface.[2−4] Nonetheless, scattering still poses a major obstacle. As the axial distance increases, the necessity to maintain high photon flux at the focus requires high incident powers, and eventually out-of-focus excitation becomes a major confounding factor, limiting imaging to no more than ∼1 mm below the tissue surface.[5]

In principle, higher-order nonlinear absorption should improve resolution at depth; however, vanishingly small multiphoton absorption cross sections of molecular chromophores have for a long time averted interest in such nonlinear methods. The break-through has become possible recently due to the advances in laser technology,[6] and the first demonstrations of three-photon (3P) imaging deep in the mouse brain have been reported.[7−17] Subsequently, 3P absorption (3PA) from a subject of purely fundamental studies in chemical physics turned into a matter of practical interest, especially in view of those applications that rely on exogenous chromophores, whose optical properties can be manipulated and optimized.

In all imaging applications, the photon wavelength preferably should be kept within the tissue transparency windows, *i.e.*, the spectral regions where the absorption by endogenous chromophores and water is minimal.[18,19] By far the most exploited windows are the regions of 650−950 and 1100−1350 nm. However, recently a window near 1700 nm has been identified as a new promising wavelength interval characterized by low endogenous absorption. This region is especially attractive for 3P microscopy,[8,11] since many chromophores possess linear (one-photon, 1P) absorption bands near 550−600 nm and potentially can be excited *via* degenerate 3PA (Figure 1) around 1700 nm.

Once within the window, the ability to selectively excite molecules near the laser focus is determined by the signal-to-

Received: September 12, 2020
Revised: November 17, 2020
Published: December 18, 2020

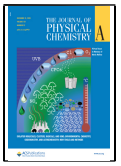

https://dx.doi.org/10.1021/acs.jpca.0c08334
J. Phys. Chem. A 2020, 124, 11038−11050

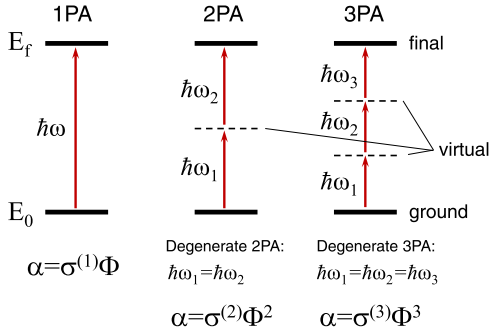

Figure 1. Energy diagram showing 1PA (linear), 2PA, and 3PA processes, *i.e.*, the absorptive transitions between the ground and final states with energies E_0 and E_f, respectively, occurring *via* one or more virtual states. When the energies of the photons are equal, the processes are called degenerate, and their respective rate constants (α, s^{-1}) are proportional to the powers of the photon flux (Φ, photons s^{-1} cm^{-2} or simply s^{-1} cm^{-2}). The proportionality coefficients $\sigma^{(1)}$, $\sigma^{(2)}$, and $\sigma^{(3)}$ are known as one-, two-, and three-proton absorption cross sections, which have the units of cm^2, s cm^4, and s^2 cm^6, respectively. For 2PA, the quantity 10^{-50} s cm^4 is defined as 1 Göeppert Mayer (GM). By analogy, in the discussion of 3PA, we will refer to the unit of 10^{-83} s^2 cm^6 as 1 GM3.

background ratio, which is proportional to the ratio of the near-focus *vs* out-of-focus absorption rate constants (α). In the case of degenerate 3PA, the rate constant scales as the cube of the photon flux (Φ), which presents the key advantage of 3PA over 2PA, in which the dependence on the flux is quadratic (Figure 1). Indeed, for a given ratio of the near-focus *vs* out-of focus fluxes (see expressions in Figure 1), the ratio of the respective rate constants increases with the order of absorption. Therefore, cubic power dependence combined with lower endogenous absorption and scattering near 1700 nm may allow imaging at depths down to ca. 2−3 mm under the tissue surface,[8,20] breaking the limits of what nonlinear microscopy methods are capable of today.

Our group has been developing the phosphorescence quenching method for biological oximetry,[21,22] which relies on exogenous metalloporphyrin-based phosphorescent probes.[23−25] Several years ago, the capabilities of the method have been extended by combining it with two-photon laser scanning microscopy. The resulting technique[26] has been proven useful in neuroscience,[27−31] stem cell biology,[32,33] cancer immunology,[34] tissue engineering,[35] ophthalmology,[36] and other areas. At present, high-resolution oxygen imaging is limited to depths not exceeding a few hundred microns,[37] which in the mouse brain corresponds to the upper levels of the cortex. Combining phosphorescence with 3PA around ∼1700 nm may allow oxygen measurements significantly deeper, possibly reaching the brain's white matter, thereby bringing new valuable physiological information. On the other hand, triplet-forming porphyrinoids present interest as sensitizers for photodynamic therapy (PDT).[38,39] 3P excitation may help to increase treatment depth, improve confinement of singlet oxygen generation to the laser focus, and thus achieve higher PDT selectivity.

While significant progress has been achieved on the instrumentation side of 3P imaging, rather scarce information exists on 3PA of organic dyes,[20,40−46] and very little is known about 3PA of porphyrins.[47,48] Porphyrins have centrosymmetric (gerade or g-) ground-state wavefunctions. According to the parity selection rules, their low-lying 1P-allowed ungerade (u-) Q and B states[49] are forbidden for 2P excitation, while the 2P-allowed g-states usually lie at such high energies that 2P excitation is overshadowed by 1PA of the vibronic states in the red tail of the Q band, or in some cases by spin-forbidden $S_0 \rightarrow T_1$ absorption to the triplet state.[50] In aromatically π-extended porphyrins, the g-states can be stabilized *via* synthetic manipulation,[51] making some of these porphyrins very strong 2P absorbers. The Pt(II) complex of one of such porphyrins, tetraaryphthalimidoporhyrin (TAPIP),[52] has been recently used to construct a high-performance two-photon oxygen probe Oxyphor 2P.[37]

In principle, parity selection rules do not impose restrictions on 3P excitation of B and Q states. However, multiphoton absorption comprises coherent action of multiple excitation channels, which may interfere constructively or destructively depending on the symmetry of the participating intermediate states. In an effort to develop detailed understanding of 3PA in porphyrins, herein we focused specifically on the class of porphyrins with aromatically extended π-system. These chromophores present particular interest for imaging due to the presence of strong absorption bands compatible with 3P excitation near 1700 nm. The 3PA spectra of several Pt complexes of porphyrins in 1200−2000 nm range were measured by the method of 3P-excited phosphorescence, derived from the technique that has been used by us previously for similar 2PA measurements.[51] To interpret the spectroscopic results, we developed a four-state model specific for porphyrins and used it in conjunction with a more quantitative computational approach,[53−56] which has already been proven successful in predicting 2PA spectra of similar porphyrinoids.[51,52] This computational method has been able to achieve excellent agreement with experiment, while the qualitative theoretical analysis allowed us to develop guidelines for future structural optimizations of porphyrins to achieve improved 3P performance.

EXPERIMENTAL METHODS

General. The synthesis and the photophysical properties of the porphyrins used in this study, including their 1PA and 2PA spectra, have been reported previously.[51,52] The solutions for optical measurements were prepared using NMR-grade dimethylformamide (DMF-d_7) and dimethyl sulfoxide (DMSO-d_6). Quartz cells (2 mm path length) were used in all optical experiments. All solutions were rigorously deoxygenated using ultrapure argon (Airgas, grade 5), as described previously.[51]

Three-Photon Absorption (3PA) Measurements. Three-photon absorption spectra in the 1200−2000 nm range were measured using the method of 3P-excited phosphorescence with time-resolved detection in time domain, which is similar to the methodology used by us previously (Section S1, Supporting Information (SI)).[51,52] Deuterated solvents and cuvettes with short optical paths were used to minimize absorption by the solvents' vibrational overtones (Section S2, SI). The excitation source was a Ti:sapphire regenerative amplifier (Coherent Libra, ∼100 fs, 800 nm, 4 W avg. power, 1 kHz rep. rate); 60% of the output of the laser was used to pump an optical parametric amplifier (OPA) to generate near-IR pulses in the 1200−2000 nm range. After passing through a series of filters (Figure S1, SI), the beam was focused in the center of a cuvette by a low-NA lens (NA 0.1, f = 4 cm). The phosphorescence was registered in a time-resolved manner using a photomultiplier tube (PMT),

https://dx.doi.org/10.1021/acs.jpca.0c08334
J. Phys. Chem. A 2020, 124, 11038−11050

positioned at 90° relative to the beam axis, and an analog-to-digital converter operating at 2 MHz frequency (National Instruments, NI-6361). At each excitation wavelength, the phosphorescence decay was integrated, and the resulting value was corrected by the incident flux and the detector quantum efficiency over the emission range. The dependence of the signal on the flux was measured throughout the spectrum to identify the regions where the absorption was purely due to the 3P mechanism and where it was contaminated by lower-order processes. In particular, we determined that near 1700−1800 nm, the power dependence was purely cubic, while near 1200 nm (Soret region), it was nearly purely quadratic. For the quantitative 3PA cross-section determination at a selected wavelength (*e.g.*, 1800 nm), the phosphorescence signals upon excitation by 3PA (1800 nm = 600 nm × 3) were compared against the signals upon excitation by 2PA (1200 nm = 600 nm × 2) using the same samples and identical optical configuration. This approach is essentially an extension of the technique used previously for the measurements of 2PA cross sections *vs* 1PA cross sections.[57] An important detail is that in our 3PA-*vs*-2PA measurements, the excitation beam was passed through a diaphragm, but kept unfocused to prevent saturation effects and the associated differences in the excitation volumes that could significantly affect the results. The 2PA cross sections of compounds **1** and **2** at the reference wavelength (1200 nm) were measured previously[51] and for **3** measured in this work. The corresponding values are 0.9 GM (**1**), 4.9 GM (**2**), 12 GM (**3**).

Quantum Chemistry Calculations. The quantum chemistry calculations were performed using in-house-modified Gaussian 09[58] in conjunction with M05-QX exchange−correlation functional.[54] The SDD Stuttgart effective core potentials were used for the metal atoms,[59] while the D95 basis set[60] was used for all other elements to prevent artificial Rydberg contributions to the valence excited states.[55,56,61] For all porphyrins, 22 excited states were calculated using time-dependent density functional theory (TDDFT). In all calculations, the solvent effects were included using the dielectric continuum model in the solvent model density (SMD) parameterization,[62] as implemented in Gaussian 09. For additional details, see ref 51.

RESULTS AND DISCUSSION

Theoretical Background. A number of theoretical papers have been published on 3PA by chromophores of different symmetries.[63−74] Here, we briefly summarize the relevant background with the purpose to construct a few-states model of 3PA specific for porphyrins, which possess certain features that are different from other centrosymmetric molecules.

3PA is the transition between an initial state, usually the ground electronic state of a molecule ψ_0, and a final state ψ_f upon nearly simultaneous action of three photons, whose combined energy must satisfy the conservation law: $\hbar\omega_1 + \hbar\omega_2 + \hbar\omega_3 = E_f - E_0$. The most practically relevant case is degenerate 3PA (Figure 1), when all three photons originate from the same laser source and have the same energy and polarization. In a qualitative picture, the first photon promotes the molecule to a virtual state (a non-eigenstate of the system), the second brings it to the second virtual state, and the third completes the process by "pushing" the molecule to the final state ψ_f.

The experimentally measured property, which quantifies the ability of an ensemble of randomly oriented molecules to undergo 3PA, is the 3PA cross section $\sigma_{0f}^{(3)}$ (Figure 1)[67,74,75]

$$\sigma_{0f}^{(3)} = \frac{16\pi^4}{n^3c^3\hbar^3}\omega_1\omega_2\omega_3\cdot\langle\delta_{0f}^{(3)}\rangle\cdot g(\omega_1+\omega_2+\omega_3) \quad (1)$$

where the subscripts 0 and f denote the transition $\psi_0 \rightarrow \psi_f$; n is the refractive index of the medium; c is the speed of light; $\hbar$ is the reduced Planck constant; ω_1, ω_2, and ω_3 are the frequencies of the photons; $g(\omega_1 + \omega_2 + \omega_3)$ is the line shape function corresponding to the transition; and $\langle\delta_{0f}^{(3)}\rangle$ is the orientationally averaged 3P transition strength. Formula 1 does not depend on the system of units.

According to McClain,[64,69] in the case of degenerate 3PA and parallel polarization of the three photons, the expression for $\langle\delta_{0f}^{(3)}\rangle$ is written as

$$\langle\delta_{0f}^{(3)}\rangle = \frac{1}{35}\sum_{\alpha,\beta,\gamma}(3T^{\alpha\alpha\beta}T^{\gamma\gamma\beta*} + 2T^{\alpha\beta\gamma}T^{\alpha\beta\gamma*}) \quad (2)$$

where $T^{\alpha\beta\gamma}$ denotes the elements of the three-photon tensor $\mathbf{T}_{0f}$. $\mathbf{T}_{0f}$ is a contravariant third-rank tensor, and for the case at hand (degenerate 3PA, parallel polarization), its elements are calculated using the following sum-over-states (SOS) expression[69]

$$T^{\alpha\beta\gamma} = \sum P_{\alpha\beta\gamma}\sum_{i,j}\left(\frac{\mu_{0i}^{\alpha}\mu_{ij}^{\beta}\mu_{jf}^{\gamma}}{(\omega_i-\omega)(\omega_j-2\omega)}\right) \quad (3)$$

where indexes α, β, and γ cycle over the Cartesian coordinates x, y, and z; $P_{\alpha\beta\gamma}$ is the permutation operator; $\sum P_{\alpha\beta\gamma}$ denotes the summation of the permutations; ω is the cyclic frequency of the photon with energy $E(\omega = E/\hbar)$; ω_i and ω_j are the frequencies corresponding to the energies of the intermediate states ψ_i and ψ_j, respectively, where indexes i and j run over all of the eigenstates of the system, including the initial and final states (ψ_0 and ψ_f); and μ_{0i}^{α}, μ_{ij}^{β}, and μ_{jf}^{γ} are the projections of the transition dipole moments for the transitions $\psi_0 \rightarrow \psi_i$, $\psi_i \rightarrow \psi_j$, and $\psi_j \rightarrow \psi_f$ on the photon's polarization axis. Here and below we omit subscripts "0f" in the notation of the tensor elements, but the relationship to the transition $\psi_0 \rightarrow \psi_f$ remains implicit.

The summation in eq 3 reflects the fact that the two virtual states on the excitation path (Figure 1) can be expanded as linear combinations in the basis of the energy eigenstates. Each term in the sum represents an excitation pathway or a channel: $\psi_0 \rightarrow \psi_i \rightarrow \psi_j \rightarrow \psi_f$ or simply $0 \rightarrow i \rightarrow j \rightarrow f$. The contribution of each channel to the sum is inversely proportional to the so-called detuning factor, *i.e.*, the difference between the energy (frequency) of the photon(s) and the energy of an intermediate state(s). The closer the energies, the larger the contribution of a channel—the effect known as resonance enhancement.

The absorption band is usually approximated by a Lorentzian shape so that in the degenerate case the value of $\sigma_{0f}^{(3)}$ at the peak of the band calculated using eq 1 becomes

$$\sigma_{0f}^{(3)} = \frac{16\pi^3}{n^3c^3\hbar^3}\omega^3\cdot\langle\delta_{0f}^{(3)}\rangle\cdot\frac{1}{\Gamma} \quad (4)$$

where Γ denotes the half-width at half-maximum (HWHM) of the Lorentzian. Thus, computing the relevant tensor elements according to eq 3, substituting them into eq 2 to obtain the

https://dx.doi.org/10.1021/acs.jpca.0c08334
J. Phys. Chem. A 2020, 124, 11038−11050

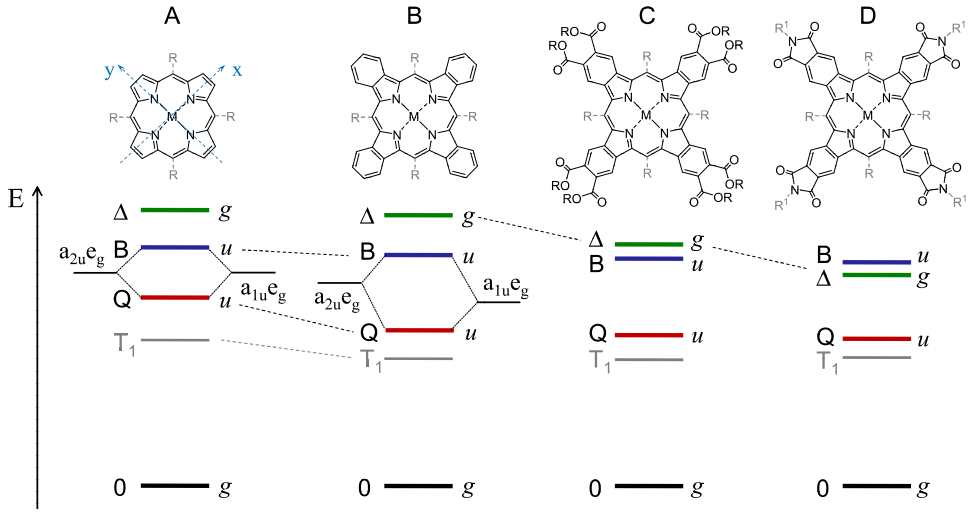

Figure 2. Effects of π-extension and substitution with electron-withdrawing groups on the energies of the lowest excited states involved in 3PA of porphyrins: (A) regular porphyrin, (B) tetrabenzoporphyrin (TBP), (C) TBP with eight ester groups in the benzo rings, (D) tetraphthalimidoporphyrin (TAPIP). Q and B (Soret) u-states are allowed for 1PA and 3PA. "0" and Δ (from Greek Δύο—two) mark the ground and the lowest 2P-allowed g-symmetry states, respectively. The Q and B states are double-degenerate and comprise pairs of orthogonally polarized transitions: Q_x, Q_y and B_x, B_y. The lowest triplet state T_1 is not involved in 3PA, but it is the origin of phosphorescence, which was used in our experimental measurements of 3PA spectra. The commonly accepted orientation of the polarization axes is shown with blue dotted lines on the structure of porphyrin A. The dotted lines in the energy diagrams mark the key changes occurring with the states' energies upon π-extension and peripheral substitution.

rotationally averaged $\langle \delta_{0f}^{(3)} \rangle$, and substituting the latter into eq 4 enable calculation of the 3PA cross section $\sigma_{0f}^{(3)}$ that can be directly compared to experiment. The main challenge is the computation of the transition dipole moments μ_{ij} connecting the excited states ($i, j \neq 0$). In this work, we used a method based on TDDFT with *a posteriori* Tamm—Dancoff approximation,[55,56,61] which has been proven successful in predicting 2PA in porphyrins.[51,52] It should be mentioned that multiple formulas for calculations of multiphoton absorption cross sections have appeared in the literature, using different systems of units, line shapes, conversion factors, etc. The formulas used in our calculations are discussed in the SI (Section S5).

The states that are most relevant to 3PA in porphyrins are shown in Figure 2. Regular nonextended symmetric porphyrins possess two quasi-degenerate highest occupied molecular orbital (HOMO)s (a_{2u} and a_{1u}) and two degenerate lowest unoccupied molecular orbital (LUMO)s (e_g).[49,76] The lowest excited states, the Q and B (Soret) states, are formed by the configuration interaction involving the single u → g excitations between these frontier orbitals. In centrosymmetric (D_{4h}) porphyrins (such as planar metalloporphyrins), the ground-state wavefunction retains its sign upon inversion of symmetry (gerade), and therefore the Q and B states are ungerade (u) states. The corresponding bands in the absorption spectra comprise two pairs of degenerate orthogonally polarized transitions, Q_x, Q_y and B_x, B_y. In D_{2h} porphyrins, such as in free-base porphyrins[76] or *cis*-dibenzo- and dinaphthoporphyrins,[77] the degeneracy is somewhat lifted, but the main spectral features are preserved. Different signs in the linear combinations of the single excitations result in the B band(s) being strongly allowed ($\varepsilon \sim 2 \times 10^5$ M^{-1} cm^{-1}) while Q band(s) quasi-forbidden ($\varepsilon \sim 10^4$ M^{-1} cm^{-1}). These are the essential features of the Gouterman's four-orbital model,[49] which underpins the porphyrin spectroscopy.

π-Extension of the porphyrin macrocycle by way of fusion of the pyrrolic fragments with external aromatic rings leads to destabilization of one of the two HOMO's (a_{1u}) relative to the other (a_{2u}).[49,78−81] As a result, the bands undergo bathochromic shifts accompanied by a redistribution of intensity: the B bands weaken and the Q bands become stronger—a phenomenon known as the intensity borrowing effect. The 2P-allowed g-states in both regular (A) and π-extended porphyrins (B), *e.g.*, tetrabenzoporphyrins (TBPs) (Figure 2), lie at rather high energies, which precludes their selective 2P excitation. However, addition of electron-withdrawing groups in the peripheral benzo-rings in TBPs (C) leads to a stabilization of the g-states, while leaving the energies of the Q and B states almost unchanged.[51] Thus, in tetraphthalimidoporphyrins (TAPIP, D), the energy of the g-state falls even below that of the B state,[52] while the B and Q bands are only slightly bathochromically shifted relative to the unsubstituted TBP (B), whose g-state remains at a significantly higher energy.

Four-State Model of 3PA in Porphyrins. To construct a qualitative model of 3PA, we assume that a porphyrin molecule is fixed, and the three photons are degenerate, plane-polarized along the *x*-axis of the macrocycle (Figure 2), that is, parallel to the Q_x and B_x transition dipole moments, and propagate in the direction perpendicular to the porphyrin plane. We consider only four states: the ground g-state, u-states Q_x and B_x, and a 2P-active g-state. We ignore the Q_y, B_y pair, as these transitions are orthogonal to the photons' polarization and neglect all of the higher-lying states based on the notion that the terms in eq 2 become smaller as the states' energies E_i increase. Hence, we refer to Q_x and B_x simply as Q and B and label the 2P-active state as Δ (from Greek Δύο—two). We also assume that all of the transitions between the excited states (Q, B, and Δ) are polarized along the *x*-axis. Under these assumptions, the numerators in the SOS expression become products of scalars μ_{ij}^x, which we denote simply as μ_{ij}. Note that in a more accurate six-state model, which will be disclosed separately, both Q_x, Q_y and B_x, B_y states are considered explicitly, and no assumptions are made about transitions' polarizations. In fact,

https://dx.doi.org/10.1021/acs.jpca.0c08334
J. Phys. Chem. A 2020, 124, 11038−11050

Table 1. Products of the Transition Dipole Moments Corresponding to the Excitation Channels in the Four-State Model of 3PA in Porphyrins

	i=0	i=Q	i=B	i=Δ
j=0	$\mu_{00}\ \mu_{00}\ \mu_{0f}$	$\mu_{0Q}\ \mu_{Q0}\ \mu_{0f}$	$\mu_{0B}\ \mu_{B0}\ \mu_{0f}$	$\mu_{0\Delta}\ \mu_{\Delta 0}\ \mu_{0f}$
j=Q	$\mu_{00}\ \mu_{0Q}\ \mu_{Qf}$	$\mu_{0Q}\ \mu_{QQ}\ \mu_{Qf}$	$\mu_{0B}\ \mu_{BQ}\ \mu_{Qf}$	$\mu_{0\Delta}\ \mu_{\Delta Q}\ \mu_{Qf}$
j=B	$\mu_{00}\ \mu_{0B}\ \mu_{Bf}$	$\mu_{0Q}\ \mu_{QB}\ \mu_{Bf}$	$\mu_{0B}\ \mu_{BB}\ \mu_{Bf}$	$\mu_{0\Delta}\ \mu_{\Delta B}\ \mu_{Bf}$
j=Δ	$\mu_{00}\ \mu_{0\Delta}\ \mu_{2\Delta}$	$\mu_{0Q}\ \mu_{Q\Delta}\ \mu_{\Delta f}$	$\mu_{0B}\ \mu_{B\Delta}\ \mu_{\Delta f}$	$\mu_{0\Delta}\ \mu_{\Delta\Delta}\ \mu_{\Delta f}$

our previous results[51] indicate that some of the transitions between the Q, B, and Δ states are polarized at an angle to one another, and the angles can vary between porphyrins. Nonetheless, here, for simplicity, we assume collinear orientation, as this will not affect our results qualitatively.

It is useful now to organize the numerators $\mu_{0i}\mu_{ij}\mu_{jf}$ in eq 2 in the form of a table, where the columns are indexed according to the first intermediate state (i) and the rows according to the second (j) (Table 1). These products of the transition dipole moments correspond to the excitation channels $0 \rightarrow i \rightarrow j \rightarrow f$, and the square of the sum of all of the products, weighted by the corresponding detuning factors, is proportional to the 3PA strength.

Based on the symmetry arguments, we can remove a number of the elements from the table. First, the transition dipole moments with two identical indexes (shown in red) are the diagonal elements of the matrix of the electric dipole operator, *i.e.*, the static (or permanent) dipole moments in the corresponding states. In centrosymmetric porphyrins, all static dipole moments are effectively zero. Second, we recall that the ground state 0 and the 2P-allowed state Δ are g-states, while the Q and B are u-states. In centrosymmetric molecules, transitions between states of equal parity (g → g or u → u) are forbidden, and hence the corresponding moments vanish as well (shown in blue). As a result, all of the elements in the table that contain colored transition dipole moments vanish, and only four terms remain.

In all of these four terms, the transitions to the final state "f" occur from the states of g-symmetry, 0 or Δ. For the corresponding moments μ_{0f} and $\mu_{\Delta f}$ to have nonvanishing values, the final state must be a u-state. Therefore, the only states allowed for 3PA are Q or B states. Combining eq 2 and Table 1, tensors elements for these transitions can be written as follows

$$T_{0Q} = -\frac{\mu_{0Q}\,\mu_{Q0}\,\mu_{0Q}}{4(\hbar\omega)^2} - \frac{\mu_{0B}\,\mu_{B0}\,\mu_{0Q}}{2\hbar\omega(E_B - \hbar\omega)} + \frac{\mu_{0Q}\,\mu_{Q\Delta}\,\mu_{\Delta Q}}{2\hbar\omega(E_\Delta - 2\hbar\omega)} + \frac{\mu_{0B}\,\mu_{B\Delta}\,\mu_{\Delta Q}}{(E_B - \hbar\omega)(E_\Delta - 2\hbar\omega)} \quad (5)$$

where $\hbar\omega = 1/3E_Q$, and

$$T_{0B} = -\frac{\mu_{0B}\,\mu_{B0}\,\mu_{0B}}{4(\hbar\omega)^2} - \frac{\mu_{0Q}\,\mu_{Q0}\,\mu_{0B}}{2\hbar\omega(E_Q - \hbar\omega)} + \frac{\mu_{0B}\,\mu_{B\Delta}\,\mu_{2B}}{2\hbar\omega(E_\Delta - 2\hbar\omega)} + \frac{\mu_{0Q}\,\mu_{Q\Delta}\,\mu_{\Delta B}}{(E_Q - \hbar\omega)(E_\Delta - 2\hbar\omega)} \quad (6)$$

where $\hbar\omega = 1/3E_B$. Here, the denominators are written in the energy scale by multiplying the corresponding denominators in eq 3 by $\hbar^2$.

Expressions 5 and 6 have four terms that correspond to the excitation channels shown in Figure 3. The first term contains

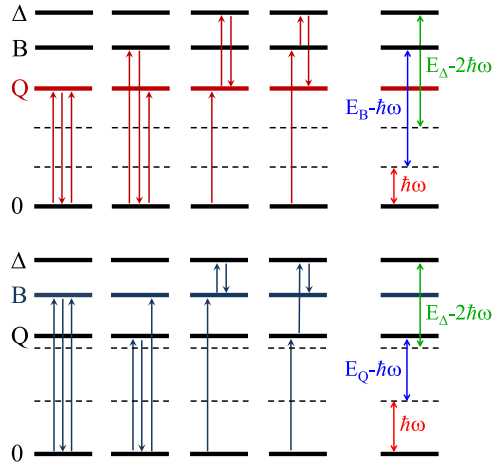

Figure 3. Diagrams illustrating the main excitation channels and the associated energies for 3PA in porphyrins.

the transitions only between the ground and final states (Q or B). The second term represents the pathway from the ground state to the final u-state involving another u-state, *e.g.*, from 0 to Q *via* B. And the last two terms represent the pathways involving one u-state and the 2P-active g-state Δ.

In all known porphyrins, the lowest excited g-states Δ have higher energies than the Q states. Therefore, for the 3PA to the Q state ($\hbar\omega = 1/3E_Q$), the conditions $E_\Delta - 2\hbar\omega > 0$ and $E_B - 2\hbar\omega > 0$ are always true, and the denominators in eq 5 are positive. In the case of the B state ($\hbar\omega = 1/3E_B$), the situation is similar. Even though in some rare cases (*e.g.*, porphyrin C in Figure 2) Δ states might occur below the B states, E_Δ is still larger than $2/3E_B$, and therefore the condition $E_\Delta - 2\hbar\omega > 0$ is also true. Similarly, even for very large Q–B gaps, E_Q is always larger than $1/3E_B$. Thus, the denominators in eq 6 are positive as well.

In general, for arbitrarily chosen initial centrosymmetric (g) and final anticentrosymmetric (u) wavefunctions, channels through intermediate u and g states exist for which the signs of the products of the transition dipole moments $\mu_{0i}\mu_{ij}\mu_{jf}$ (or their projections) may be different, depending on the choice of these states. However, calculations reveal that in porphyrins A–D (Figure 2), the products $\mu_{0i}\mu_{ij}\mu_{jf}$, connecting the ground

https://dx.doi.org/10.1021/acs.jpca.0c08334
J. Phys. Chem. A 2020, 124, 11038–11050

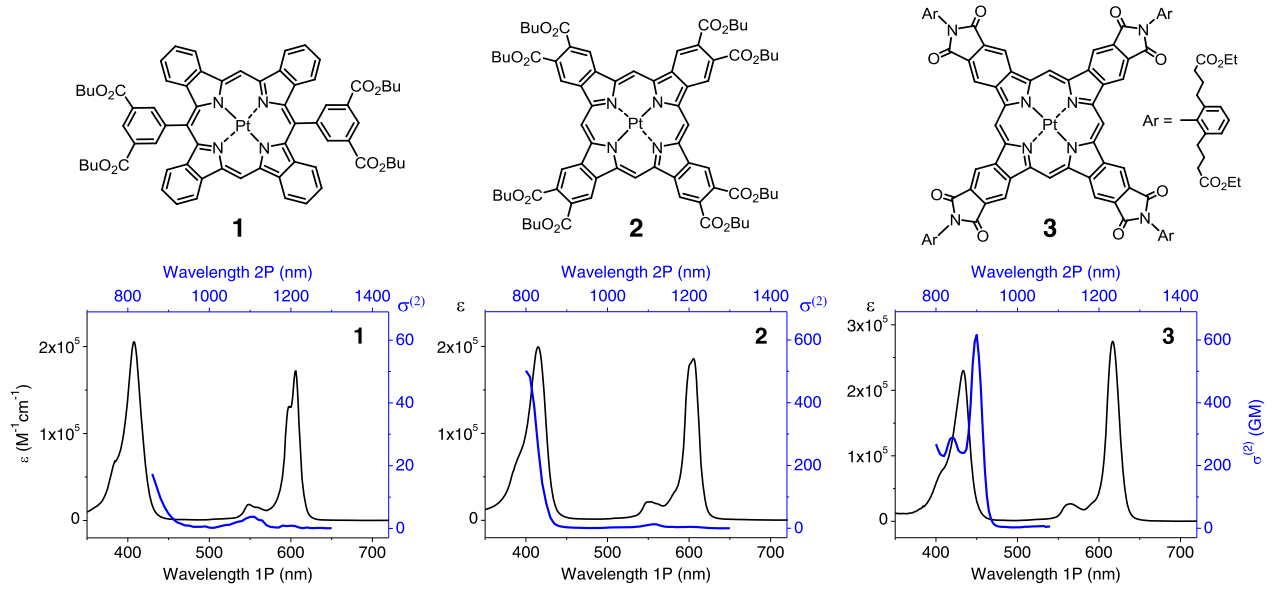

Figure 4. Structures of the studied Pt porphyrins **1**−**3** and their 1P and 2P absorption spectra in dimethylformamide (DMF).

state (0) and the final state (f) Q or B *via* intermediate states *i* and *j*, where *i* = Q or B and *j* = 0 or Δ, always have the same sign. Since the numerators have the same sign and the denominators also have the same (positive) sign, the signs of the first two terms and the last two terms in Expressions 5 and 6 are the opposite. Consequently, these pairs of the excitation channels are said to interfere destructively.

The extent of the destructive interference depends on the actual values of the transition dipole moments μ_{0Q}, μ_{0B}, $\mu_{\Delta Q}$, and $\mu_{\Delta B}$ (it is implicit that all of the eigenstates and, consequently, the transition dipole moments are real so that $\mu_{0Q} = \mu_{Q0}$, $\mu_{0B} = \mu_{B0}$, etc.), and a priori, it is impossible to tell which pathways have larger amplitudes. If the terms involving state Δ are dominant, then further increasing their amplitudes would lead to an overall increase in $\delta^{(3)}$. Conversely, if the combined magnitude of the first two terms is larger, then increasing the contribution of the pathways involving state Δ, *e.g.*, by lowering its energy, will, up to a point, lead to a decrease in $\delta^{(3)}$. The calculations (see below) reveal that for the group of porphyrins studied in this work, the second scenario is the one that actually takes place, *i.e.*, the stronger the Q → Δ and B → Δ transitions and the lower the energy E_Δ, the more the channels involving state Δ act to decrease the 3PA strength $\delta^{(3)}$. An illustration of this effect reflecting the situation in tetrabenzoporphyrins (Figure 2B−D) is shown in Figure S2.

Experimental 3PA Spectra. The structures and the 1PA and 2PA spectra of Pt porphyrins **1**−**3** studied in this work are shown in Figure 4, and their phosphorescence spectra scaled by the emission quantum yields are shown in Figure 5.

Pt porphyrins **1**−**3** have been described previously.[51,52] They belong to the group of π-extended porphyrins of types B−D (Figure 2). Due to the presence of Pt(II) ions, spin−orbit coupling in these porphyrins is very strong, and the triplet states form with nearly unity efficiency.[82,83] All three compounds phosphoresce in deoxygenated solutions at ambient temperatures with emission decay times in the range of 30−50 μs.

Based on X-ray crystal analysis and structural calculations,[52,84] the macrocycles in **2** and **3** are practically flat. But in

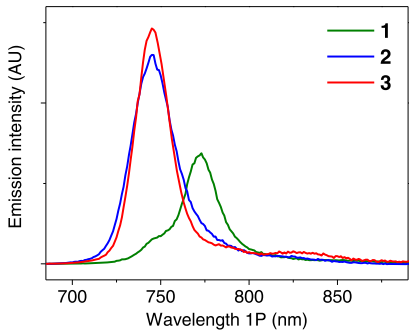

Figure 5. Phosphorescence spectra of porphyrins **1**−**3** (DMF deox, 22 °C). The integrated intensities of the spectra were scaled by the respective emission quantum yields: 0.23 (**1**), 0.45 (**2**), 0.45 (**3**).

1, the macrocycle is slightly distorted, both in- and out-of-plane, due to the *meso*-aryl groups with pendant butoxycarbonyl moieties. The latter were appended to the porphyrin to enhance its solubility. These *meso*-aryl groups are nearly orthogonal to the macrocycle, but still are partially conjugated with its electronic system, effectively lowering its symmetry. However, this effect is not large.

Compared to **1**, porphyrins **2** and **3** possess peripheral electron-withdrawing substituents directly in the benzo-rings. In **3**, the carbonyl groups are fixed in-plane with the macrocycle, while in **2**, the ester moieties can rotate, and at the energy minimum, the carbonyls are tilted out of plane by ∼40°. As a result, their conjugation with the macrocycle is weakened. These differences are manifested by several spectroscopic features. First, the presence of the peripheral substituents in **2** and **3** *vs* **1** and their stronger conjugation in **3** *vs* **2** lead to a progressive destabilization of a_{1u} HOMO throughout the series (Figure 2). The destabilization increases the intensity-borrowing effect so that in **3**, the Q band has an even greater intensity than the B band (ε_Q = 275 000 M^{-1} cm^{-1} *vs* ε_B = 242 000 M^{-1} cm^{-1}).[52] Second, the peripheral groups have the most pronounced effect on the energy of the 2P-active state Δ, which decreases throughout the series and in compound **3** reaches even lower than the B state level (Figures 2 and 4). Note that the 2PA spectra of **1** and **2** (Figure 5) are

https://dx.doi.org/10.1021/acs.jpca.0c08334
J. Phys. Chem. A 2020, 124, 11038−11050

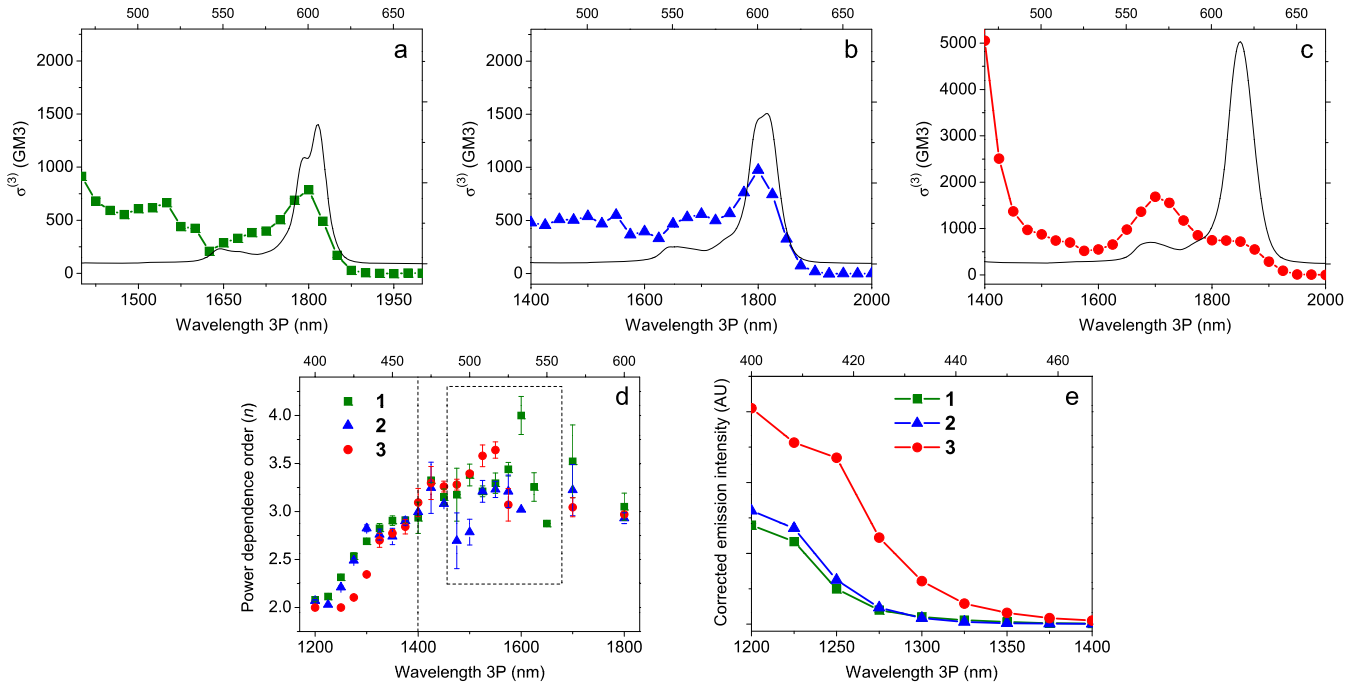

Figure 6. Three-photon absorption spectra of the studied porphyrins: (a) **1** (DMF-d_7), (b) **2** (DMF-d_7), (c) **3** DMSO-d_6. 1 GM3 = 10^{-83} cm^6 s^2. The linear (1P) absorption spectra are shown by thin black lines along with the respective wavelength scales (top). (d) Order of power dependence (m) in the range of 1200−2000 nm. Below 1400 nm (dashed line), m steeply changes from 3 to 2. Therefore, 3PA cross sections ($\sigma^{(3)}$) are reported only in the range 1400−2000 nm (a−c). (e) Relative emission intensities due to mixed 3PA/2PA (normalized by the emission quantum yields, concentration, detector sensitivity, and flux-cubed, assuming pure 3PA mechanism).

Table 2. Experimental Spectroscopic and Photophysical Data for Porphyrins 1−3[a]

compd no.	λ_{max} Q λ_{max} B (nm)	E_{max} Q E_{max} B (eV)	ε_{max} Q ε_{max} B (cm^{-1} M^{-1})	f[b]	λ_{max} p[c] (nm)	ϕ_p[d]	λ_{max} 2P[e] (nm)	$\sigma_{max}^{(2)}$[f] (GM)	λ_{max} 3P[g] (nm)	$\sigma_{max}^{(3)}$[h] (GM3)[i]
1	605	2.05	168 120	0.50	771	0.23	864	17	1800	790
	407	3.05	205 450	1.67						
2	605	2.05	184 790	0.62	743	0.45	800	503	1800	970
	415	2.99	199 580	1.77						
3	616	2.01	274 700	0.78	744	0.45	900	616	1700	1690
	433	2.86	242 500	1.84						

[a]All 1P and 2P measurements were performed in dimethylacetamide (DMA) at 22 °C. 3P measurements were performed in DMF-d_7 (**1**, **2**) or DMSO-d_6 (**3**). [b]f is oscillator strength. [c]"p" represents phosphorescence. [d]ϕ_p is the phosphorescence quantum yield. [e]λ_{max} 2P is the wavelength corresponding to the maximal value of $\sigma^{(2)f}$ in the spectrum. [f]$\sigma_{max}^{(2)}$ is the maximal measured value of the 2PA cross section. [g]λ_{max} 3P is the wavelength corresponding to the maximal value of $\sigma^{(3)j}$ in the Q band region (Figure 6a−c). [h]$\sigma_{max}^{(3)}$ is the maximal value of the 3PA cross section in the Q band region. [i]1 GM3 = 10^{-83} cm^6 s^2.

truncated before reaching their respective maxima. The blue edges in these spectra are set by the interfering spin-forbidden 1P excitation directly to the triplet state ($S_0 \rightarrow T_1$),[51] which prevents observation of the true 2PA peaks.

The 3PA spectra of porphyrins **1**−**3** are shown in Figure 6a−c, and the relevant spectroscopic and photophysical data are summarized in Table 2. The measurements were performed in the region of 1200−2000 nm, and at each wavelength the order of absorption was assessed by recording the dependence of the phosphorescence signal on the excitation flux (Figure 6d). In the interval ca. 1450−1650 nm, the measurements were noisy due to the instability of the OPO near the energy minima for both the signal and the idler; but overall above 1400 nm, the absorption order (m) on average was ∼3. Below 1400 nm, the signals strongly intensified (Figure 6e); however, m steeply dropped and became ∼2 near 1200 nm (Section S4, SI). Indeed, for all of the studied compounds, the laser wavelength corresponding to the 3PA peak in the B region practically coincides with the wavelength corresponding to the 2PA peak in the Q region. Although the Q state is forbidden for 2PA, some vibronic transitions in the Q band envelope still exhibit nonzero 2P strength.[51] Because 2PA is a much more probable process even for very small cross sections $\sigma^{(2)}$, it completely overshadows 3PA near 1200 nm, where both 2P and 3P excitations (of Q and B states, respectively) are energetically feasible. Therefore, $\sigma^{(3)}$ values are reported in Figure 6a−c only for the interval 1400−2000 nm. It is worth mentioning that for practical purposes, carrying out excitation below 1400 nm may still be beneficial due to much higher signal strengths (Figure S5), notwithstanding some losses in the order of nonlinearity.

To the best of our knowledge, the data reported in Figure 6 present the first example of 3PA spectra of porphyrins in the Q band region. The absolute values of the cross sections at the

https://dx.doi.org/10.1021/acs.jpca.0c08334
J. Phys. Chem. A 2020, 124, 11038−11050

Table 3. Calculated Energies (E), Transition Dipole Moments (μ), 3PA Cross Sections ($\sigma^{(3)}$), and Fractional Contributions ($\sum$) of the Channels Involving States 0, Q, B, and Δ to the Total Transition Strength ($\delta^{(3)}$) for Degenerate 3P Excitation of the Q States in Porphyrins 1−3

	E_Q (eV)		$\lvert\mu_{0Q}\rvert$ (D)	$\lvert\mu_{Q\Delta}\rvert$ (D)							
compd no.	E_B (eV)[a]	E_Δ (eV)[b]	$\lvert\mu_{0B}\rvert$ (D)[c]	$\lvert\mu_{B\Delta}\rvert$ (D)[c]	$\sigma_{calc}^{(3)}$ (GM3)[d]	$\sigma_{expt}^{(3)}$ (GM3)[e]	$\sigma_{calc}^{(3)}/\sigma_{expt}^{(3)}$[f]	$\sum_0$[g]	$\sum_Q$[g]	$\sum_B$[g]	$\sum_\Delta$[g]
1	2.28	3.77	2.63	0.46	1772	788	2.25	0.51	0.16	0.33	−0.01
	3.29		3.96	0.18							
2	2.27	3.47	2.93	2.06	2394	974	2.46	0.57	0.19	0.31	−0.07
	3.17		4.46	1.03							
3	2.22	2.98	3.29	2.19	3938	1687	2.33	0.59	0.21	0.29	−0.09
	3.02		4.45	1.49							

[a]Only the energies of the Q_x and B_x states are shown. The energies of the Q_y and B_y states are very close.[51,52] [b]Energies of the lowest 2P-active g-states Δ.[51,52] [c]Transition dipole moments' lengths for the Q_x and B_x transitions are shown. The moments' lengths corresponding to the Q_y and B_y transitions are very close.[51,52] [d]$\sigma_{calc}^{(3)}$ is the sum of the calculated 3PA cross sections for the Q_x and Q_y transitions. [e]$\sigma_{expt}^{(3)}$ is the maximal experimental value of the 3PA cross section in the Q band region. 1 GM3 = 10^{-83} cm^6 s^2. [f]Ratio of the calculated and experimental 3PA cross sections. [g]The fraction of the contributions of the channels involving the respective state (Q, B, or Δ) to the total 3P strength. The contributions of the higher excited states were found to be less than 0.01 and thus are not included in the table.

maxima were found to be on the order of 1000 GM3 (1 GM3 = 10^{-83} cm^6 s^2) for all of the compounds, while porphyrin **3** was found to be the strongest absorber in the series with $\sigma_{max}^{(3)}$ = 1678 GM3. This value compares very favorably with cross sections of other organic dyes. For example, the action cross section ($\sigma_a^{(3)}$) of SR101 (sulforhodamine 101) at 1700 nm ($\sigma_a^{(3)} = \sigma^{(3)} \times \phi$, where ϕ is the emission quantum yield) was reported to be 6.5 GM3,[20] which translates into $\sigma^{(3)} \approx 7.3$ GM3 (ϕ_{fl} = 0.95 of SR101 in EtOH).[85] The 3PA cross section of porphyrin **3** is more than 2 orders of magnitude higher. Given that optical probes based on SR101 have already been applied successfully in 3P microscopy,[8] more than 200 times higher cross section obviously makes **3** an excellent candidate for similar imaging applications. In this regard, the maximum of the 3PA spectrum of **3** corresponds to the 0−1 vibronic transition (note the difference with the 1PA spectrum), which is positioned exactly at 1700 nm, *i.e.*, the minimum of tissue absorption in the corresponding biological window.[18,19]

It is important to mention that 3PA measurements by way of 3P excitation spectra may be confounded by another interfering nonlinear pathway having the same cubic power dependence as 3PA, namely, third-harmonic generation (THG), followed by regular linear absorption, THG → 1PA. Unlike second-harmonic generation, THG can occur in isotropic symmetric medium, and it is known to be enhanced at refractive index interfaces (*e.g.*, near optical cell walls),[86,87] which has been successfully used in the development of THG microscopy.[88−90] However, in our experiments, the aforementioned pathway likely did not play a significant role. THG typically requires tight spatial focusing of the laser beam, while in our 3PA quantification experiments (performed by comparison of 3PA-induced emission with that induced by 2PA), the beam was collimated and directed perpendicular to the optical cell wall. More importantly, the shapes of the measured 3PA spectra are distinctly different from those of the 1PA spectra (see, for example, Figure 6c, compound **3**). If the excitation would be dominated by the THG → 1PA pathway, one would expect 3PA and 1PA spectra to have nearly identical profiles.

A possibility also exists that the origin of THG are the solute molecules themselves, whereby interaction of the optical field with a porphyrin would result in THG with emission of a photon, which would be subsequently absorbed by another porphyrin molecule and emitted as phosphorescence. The SOS expressions describing the third-order susceptibilities for THG and 3PA are similar in terms of their resonance structures.[75] Therefore, ruling out the THG-based pathways based on the difference between the 3PA and 1PA spectra would be difficult. Nevertheless, to obtain appreciable resonance enhancement of THG by solute molecules, the latter would usually need to be taken in millimolar concentrations, that is, ∼100 higher than in our measurements, and the experiments would typically involve irradiation of a solution interface by a highly focused laser beam.[91] In the future, it will be interesting to directly compare the efficiencies of 3PA and THG → 1PA pathways, particularly in spatially inhomogeneous systems under focused irradiation, as both of them can effectively contribute to nonlinear excitation in microscopy applications.

Since the 3PA measurements below 1400 nm were obstructed by the interfering 2PA, quantitative interpretation of the experimental data is warranted only for the Q band region. The increase in $\sigma^{(3)}$ in the series is consistent with the increase in the oscillator strength of both Q and B transitions (Table 2) and consequently with a rise of the absolute values of the first two terms in expression 5. On the other hand, the energy of the 2P-active state Δ decreases from **1** to **3** and that leads to an increase in the last two terms due to the resonance enhancement effect. As mentioned above, the first two terms and the second two terms counteract, but which pair increases $\sigma^{(3)}$ and which dampens it depend on their absolute magnitudes of these terms.

To quantify the observed trends, we carried out calculations of the 3PA spectra of porphyrins **1**−**3** using the DFT/TDDFT/ATDA method[55,56] coupled with the SOS formalism. The details of the calculations (orbitals, states energies, oscillator strengths, 2PA cross sections, etc.) can be found in the previous publications.[51,52] In this work, the 3PA spectra were computed using the first 10 excited states. It was found that addition of more states did not significantly affect the results. The calculations were performed using full orientational averaging assuming an ensemble of randomly oriented molecules excited by three degenerate linearly polarized photons. The formulas for the calculations of the 3P tensor elements and the 3PA cross sections can be found in the SI (Section S5). The summary of the computational results is given in Table 3.

First, we note a rather good agreement between the computational and experimental results. The computed cross

https://dx.doi.org/10.1021/acs.jpca.0c08334
J. Phys. Chem. A 2020, 124, 11038−11050

section values are overestimated approximately 2-fold, but all of the trends are reproduced correctly. The ∼2-fold difference may arise from the choice of parameters in the formulas for calculation of the cross sections (see Section S5, SI). Previously, we have found that the method used in this and our previous work for computing transition dipole moments between the excited states, which underpins calculations by the SOS formulas, is capable of accurate predictions of 2PA spectra of porphyrins. The present result further enhances confidence in this methodology as a tool for evaluation of multiphoton absorption cross sections of porphyrins and similar chromophores.

Using expressions for the 3P tensor elements, it is possible to quantify the fraction of the contribution of each excitation channel to the total transition strength $\delta^{(3)}$. For example, within the framework of our four-state model, we can rewrite expression 5 for 3PA to the Q state as follows

$$T_{0Q} = \sum_{m}^{N} p_m \quad \text{and}$$
$$\delta_{0Q}{}^{(3)} = T_{0Q}{}^{2} = \sum_{m,n}^{N} p_m p_n = \sum_{m}^{N} p_m^2 + 2\sum_{n>m}^{N} p_m p_n \tag{7}$$

where p_m represents the individual terms in eq 5, taken with their respective signs, and indexes m and n run from 1 to N = 4. The fractional contribution θ_k of each channel can now be defined as

$$\theta_k = \frac{p_k^2 + \sum_{n\neq k}^{N} p_k p_n}{T_{0Q}{}^{2}}, \quad \sum_{k}^{N} \theta_k = 1 \tag{8}$$

By adding contributions θ_k's of all of the channels $0 \rightarrow i \rightarrow j \rightarrow f$ in which state ψ appears as an intermediate state (either i or j), weighted by the numbers of times that these pathways are counted in the sums, the total contribution of the channels encompassing state ψ, $\sum_{\psi}$, can be calculated. For example, the Q state appears in eq 5 as an intermediate state in the terms p_1 and p_3, but each of these terms also involves another intermediate state, 0 and Δ, respectively. Hence, each channel will be counted twice, and the contribution of all channels involving the Q state, or simply the contribution of the Q state, should be calculated as

$$\sum_{Q} = \frac{\theta_1}{2} + \frac{\theta_3}{2} \tag{9}$$

It is easy to see that using this definition, the sum of the contributions of all states is 1. Similar albeit slightly more bulky expressions can be readily obtained for complete orientational averaging and arbitrary number of states (Section S6, SI). These expressions were used in our analysis of the contributions of states 0, B, Q, and Δ that are shown in Table 3.

When considering 3P excitation to the lowest excited state of a molecule, it is common to approximate the 3PA strength $\delta^{(3)}$ using a simple two-state model,[69] which takes into account only the initial and final states. For dyes that have single intense transition to the lowest excited state, with other states lying at substantially higher energies, such an approximation is generally appropriate. However, our results clearly show that in the case of porphyrins, the B state, which is located relatively close to the Q state energetically and is typically associated with higher oscillator strength, cannot be neglected. It is seen in Table 3 that the combined contribution of the channels encompassing the B state to the Q transition is even larger than the contribution of the Q state itself. The contribution of the latter increases throughout the series, while the contribution of the B state drops, reflecting the increase in the intensity-borrowing effect. It is worth mentioning that the B state was found earlier to play a major role in 2PA to the state Δ in porphyrins as well by acting along with the Q state and providing as much as 30% of the transition amplitude.[51,52] Thus, the B state in spite of its higher energy is a key player in multiphoton absorption of porphyrins and should be considered in all few-states models.

The calculations also reveal that the transition dipole moments connecting the B and Q states with the 2P-active state Δ ($\mu_{Q\Delta}$ and $\mu_{B\Delta}$) increase throughout the series, but in all cases remain smaller than the moments μ_{0Q} and μ_{0B}, and consequently, the terms in expression 5 that involve state Δ have lower magnitudes. Therefore, state Δ effectively acts to reduce the 3PA strength. This result might seem counter-intuitive first, since the presence of a low-lying g-state would be expected to create additional excitation channels between the ground and final states and thus increase the transition probability. Nevertheless, because the products of the transition dipole moments in all four terms in eq 5 have the same sign, but the energies of the states happened to be such that the signs of the first two terms and the last two terms are the opposite, the combined effect of the channels involving state Δ is overall negative.

The largest fraction of the transition strength in all porphyrins is due to the ground state. This is not surprising, because neither Q nor B states cannot create excitation channels independently, but must act in conjunction with a g-state. In fact, we can see in Table 3 that when the negative contribution of state Δ is small (*e.g.*, porphyrin **1**) the combined contributions $\sum_{B}$ and $\sum_{Q}$ are almost the same as that of the ground state $\sum_{0}$, and in all cases, the combined contributions of all u-states and all g-states are equal.

The counteracting interference of the channels involving state Δ increases throughout the series, and yet porphyrin **3** has the highest 3PA cross section among the three molecules. Apparently, the increase in the moments μ_{0Q} and μ_{0B} along with the narrowing of the B−Q energy gap, which intensifies the resonance enhancement of the second term, overpowers the negative effect of the g-state, and the overall transition strength increases.

The special features of the electronic structure of π-extended porphyrins explain why these molecules exhibit such high values of effective 3PA cross sections compared to, *e.g.*, SR101[20] and most other small molecules[20,40] as well as fluorescent proteins.[41] Not only that the oscillator strengths of their lowest energy bands (Q-bands) are unprecedentedly high, but in addition, they possess the second excited state, the B (Soret) state, which has the same electronic origin as the Q state, lies relatively low in energy, and effectively assists 3PA to the Q state. Such states are absent in SR101 and similar dyes.

The above analysis illustrates the complex interplay of factors that underlie 3PA in porphyrins and suggests ways in which their electronic structure can be manipulated to achieve 3P maximal efficiency. First, the oscillator strengths of the Q and B transitions should be maximized—a general strategy pointed out earlier for centrosymmetric molecules.[68,69,72] Such boost in absorbance may be achieved *via* π-extension and/or

https://dx.doi.org/10.1021/acs.jpca.0c08334
J. Phys. Chem. A 2020, 124, 11038−11050

peripheral substitution. Second, one should avoid low-lying g-states and the associated strong Q → Δ and B → Δ transitions that interfere negatively in the 3PA process. On the other hand, one could, in principle, envision a situation where the energy of the g-state Δ is so low ($E_\Delta < 2\hbar\omega$) that the signs of the latter two terms in expression 5 flip, and instead of interfering destructively, the Δ state would be contributing positively to 3PA. Porphyrinoids with such low-lying g-states are presently unknown, and the energies of 2P-states in porphyrins are not easy to predict based on the existing structure−property relationships; however, as we have shown in this work, the latter may be assessed computationally and used in the evaluation of 3PA properties.

CONCLUSIONS

In this work, the 3PA spectra of several porphyrins were measured for the first time. The analysis of the spectra using a qualitative four-state model and quantum chemical calculations revealed the following general trends: (1) in porphyrins 3P transitions to the lowest excited states (the Q states) are significantly enhanced by the B (Soret) states, which create excitation channels that are collectively responsible for a large fraction of contribution to the overall 3P strength; (2) in contrast, the "hidden" 2P-active excited states (Δ) interfere negatively in the excitation process and diminish the 3P strength; and (3) the latter negative interference becomes larger as the energy of the Δ drops. Nonetheless, in the series of the porphyrins studied in this work, the increase in the negative contribution of the g-state Δ was overpowered by the increasing contribution of the competing positive channels. This analysis should facilitate development of porphyrins with improved 3PA performance.

On the practical side, the effective 3PA cross sections of the studied molecules were found to be among the highest known in the near-infrared spectral range[20,40,41,43] and the highest in the region of 1700 nm—a newly emerged tissue transparency window.[18,19] Here, we should note that a number of rather high 3PA cross-section values for various chromophores have been measured by the *Z*-scan method.[44,45] However, the latter technique is known to routinely overestimate cross sections compared to luminescence excitation techniques.[92] Combined with the fact that some of the studied porphyrins are already used as functional units in the biological probes for oxygen, the present results suggest that these sensors may be applied directly to measure tissue oxygenation by means of 3P microscopy, potentially overcoming the existing depth limitations and bringing new physiological information not obtainable by any other methods. Specifically, in relation to neuroimaging, the investigated molecules, which combine exceptionally large 3PA cross sections with high phosphorescence quantum yields, should provide a valuable tool for probing oxygen metabolism at depths beyond the brain cortical area. The corresponding experiments are currently underway.

ASSOCIATED CONTENT

Supporting Information

The Supporting Information is available free of charge at https://pubs.acs.org/doi/10.1021/acs.jpca.0c08334.

Additional experimental details, optical spectroscopic data, and formulas for calculations (PDF)

AUTHOR INFORMATION

Corresponding Author

Sergei A. Vinogradov − *Department of Biochemistry and Biophysics, Perelman School of Medicine, University of Pennsylvania, Philadelphia, Pennsylvania 19104, United States; Department of Chemistry, School of Arts and Sciences, University of Pennsylvania, Philadelphia, Pennsylvania 19104, United States;* orcid.org/0000-0002-4649-5534; Email: vinograd.upenn@gmail.com

Authors

Luca Ravotto − *Department of Biochemistry and Biophysics, Perelman School of Medicine, University of Pennsylvania, Philadelphia, Pennsylvania 19104, United States; Department of Chemistry, School of Arts and Sciences, University of Pennsylvania, Philadelphia, Pennsylvania 19104, United States*

Stephen L. Meloni − *Department of Chemistry, School of Arts and Sciences, University of Pennsylvania, Philadelphia, Pennsylvania 19104, United States*

Tatiana V. Esipova − *Department of Biochemistry and Biophysics, Perelman School of Medicine, University of Pennsylvania, Philadelphia, Pennsylvania 19104, United States; Department of Chemistry, School of Arts and Sciences, University of Pennsylvania, Philadelphia, Pennsylvania 19104, United States*

Artëm E. Masunov − *NanoScience Technology Center, Department of Chemistry, and School of Modeling, Simulation and Training, University of Central Florida, Orlando, Florida 32826, United States; National Nuclear Research University MEPhI, Moscow 115409, Russia; South Ural State University, Chelyabinsk 454080, Russia;* orcid.org/0000-0003-4924-3380

Jessica M. Anna − *Department of Chemistry, School of Arts and Sciences, University of Pennsylvania, Philadelphia, Pennsylvania 19104, United States;* orcid.org/0000-0001-5440-6987

Complete contact information is available at: https://pubs.acs.org/10.1021/acs.jpca.0c08334

Notes

The authors declare no competing financial interest.

ACKNOWLEDGMENTS

Support of the grants R24NS092986, EB027397, and U24EB028941 from the National Institutes of Health (S.A.V.); the Alfred P. Sloan Foundation and startup funds from the University of Pennsylvania (J.M.A.); the "Improving of the Competitiveness" program of the National Nuclear Research University "MEPhI" and by the Act 211 of the Government of the Russian Federation (Contract no. 02.A03.21.0011) (A.E.M.); and the T32 predoctoral training grant GM008275 from the NIH (S.L.M.) is gratefully acknowledged. Computations were performed using the computational resource at the Department of Biochemistry of Biophysics (UPenn), funded by the grant S10-OD023592 from the NIH and by the Johnson Research Foundation.

REFERENCES

(1) Denk, W.; Strickler, J. H.; Webb, W. W. Two-photon laser scanning fluorescence microscopy. *Science* **1990**, *248*, 73−76.
(2) Hoover, E. E.; Squier, J. A. Advances in multiphoton microscopy technology. *Nat. Photonics* **2013**, *7*, 93−101.

(3) Helmchen, F.; Denk, W. Deep tissue two-photon microscopy. *Nat. Methods* **2005**, *2*, 932−940.
(4) Xu, C.; Zipfel, W.; Shear, J. B.; Williams, R. M.; Webb, W. W. Multiphoton fluorescence excitation: New spectral windows for biological nonlinear microscopy. *Proc. Natl. Acad. Sci. U.S.A.* **1996**, *93*, 10763−10768.
(5) Theer, P.; Hasan, M. T.; Denk, W. Two-photon imaging to a depth of 1000 μm in living brains by use of a Ti:Al_2O_3 regenerative amplifier. *Opt. Lett.* **2003**, *28*, 1022−1024.
(6) Lefort, C. A review of biomedical multiphoton microscopy and its laser sources. *J. Phys. D: Appl. Phys.* **2017**, *50*, No. 423001.
(7) Chow, D. M.; Sinefeld, D.; Kolkman, K. E.; Ouzounov, D. G.; Akbari, N.; Tatarsky, R.; Bass, A.; Xu, C.; Fetcho, J. R. Deep three-photon imaging of the brain in intact adult zebrafish. *Nat. Methods* **2020**, *17*, 605−608.
(8) Horton, N. G.; Wang, K.; Kobat, D.; Clark, C. G.; Wise, F. W.; Schaffer, C. B.; Xu, C. *In vivo* three-photon microscopy of subcortical structures within an intact mouse brain. *Nat. Photonics* **2013**, *7*, 205−209.
(9) Lanin, A. A.; Pochechuev, M. S.; Chebotarev, A. S.; Kelmanson, I. V.; Bilan, D. S.; Kotova, D. A.; Tarabykin, V. S.; Ivanov, A. A.; Fedotov, A. B.; Belousov, V. V.; et al. Cell-specific three-photon-fluorescence brain imaging: neurons, astrocytes, and gliovascular interfaces. *Opt. Lett.* **2020**, *45*, 836−839.
(10) Miller, D. R.; Hassan, A. M.; Jarrett, J. W.; Medina, F. A.; Perillo, E. P.; Hagan, K.; Shams Kazmi, S. M.; Clark, T. A.; Sullender, C. T.; Jones, T. A.; et al. *In vivo* multiphoton imaging of a diverse array of fluorophores to investigate deep neurovascular structure. *Biomed. Opt. Express* **2017**, *8*, 3470−3481.
(11) Miller, D. R.; Jarrett, J. W.; Hassan, A. M.; Dunn, A. K. Deep tissue imaging with multiphoton fluorescence microscopy. *Curr. Opin. Biomed. Eng.* **2017**, *4*, 32−39.
(12) Ouzounov, D. G.; Wang, T.; Wang, M.; Feng, D. D.; Horton, N. G.; Cruz-Hernandez, J. C.; Cheng, Y. T.; Reimer, J.; Tolias, A. S.; Nishimura, N.; et al. *In vivo* three-photon imaging of activity of GCaMP6-labeled neurons deep in intact mouse brain. *Nat. Methods* **2017**, *14*, 388−390.
(13) Tong, S.; Liu, H.; Cheng, H.; He, C.; Du, Y.; Zhuang, Z.; Qiu, P.; Wang, K. Deep-brain three-photon microscopy excited at 1600 nm with silicone oil immersion. *J. Biophotonics* **2019**, *12*, No. e201800423.
(14) Wang, T.; Ouzounov, D. G.; Wu, C.; Horton, N. G.; Zhang, B.; Wu, C. H.; Zhang, Y.; Schnitzer, M. J.; Xu, C. Three-photon imaging of mouse brain structure and function through the intact skull. *Nat. Methods* **2018**, *15*, 789−792.
(15) Wang, Y.; Chen, M.; Alifu, N.; Li, S.; Qin, W.; Qin, A.; Tang, B. Z.; Qian, J. Aggregation-induced emission luminogen with deep-red emission for through-skull three-photon fluorescence imaging of mouse. *ACS Nano* **2017**, *11*, 10452−10461.
(16) Yildirim, M.; Sugihara, H.; So, P. T. C.; Sur, M. Functional imaging of visual cortical layers and subplate in awake mice with optimized three-photon microscopy. *Nat. Commun.* **2019**, *10*, No. 177.
(17) Liu, H.; Deng, X.; Tong, S.; He, C.; Cheng, H.; Zhuang, Z.; Gan, M.; Li, J.; Xie, W.; Qiu, P.; et al. *In vivo* deep-brain structural and hemodynamic multiphoton microscopy enabled by quantum dots. *Nano Lett.* **2019**, *19*, 5260−5265.
(18) Tuchin, V. V. Tissue optics and photonics: light-tissue interaction. *J. Biomed. Photonics Eng.* **2015**, *1*, 98−134.
(19) Shi, L.; Sordillo, L. A.; Rodriguez-Contreras, A.; Alfano, R. Transmission in near-infrared optical windows for deep brain imaging. *J. Biophotonics* **2016**, *9*, 38−43.
(20) Cheng, L. C.; Horton, N. G.; Wang, K.; Chen, S. J.; Xu, C. Measurements of multiphoton action cross sections for multiphoton microscopy. *Biomed. Opt. Express* **2014**, *5*, 3427−3433.
(21) Vanderkooi, J. M.; Maniara, G.; Green, T. J.; Wilson, D. F. An optical method for measurement of dioxygen concentration based on quenching of phosphorescence. *J. Biol. Chem.* **1987**, *262*, 5476−5482.
(22) Rumsey, W. L.; Vanderkooi, J. M.; Wilson, D. F. Imaging of phosphorescence: a novel method for measuring oxygen distribution in perfused tissue. *Science* **1988**, *241*, 1649−1651.
(23) Lebedev, A. Y.; Cheprakov, A. V.; Sakadzic, S.; Boas, D. A.; Wilson, D. F.; Vinogradov, S. A. Dendritic phosphorescent probes for oxygen imaging in biological systems. *ACS Appl. Mater. Interfaces* **2009**, *1*, 1292−1304.
(24) Esipova, T. V.; Karagodov, A.; Miller, J.; Wilson, D. F.; Busch, T. M.; Vinogradov, S. A. Two new "protected" oxyphors for biological oximetry: properties and application in tumor imaging. *Anal. Chem.* **2011**, *83*, 8756−8765.
(25) Vinogradov, S. A.; Wilson, D. F. Porphyrin-Dendrimers as Biological Oxygen Sensors. In *Designing Dendrimers*; Capagna, S.; Ceroni, P., Eds.; Wiley: New York, 2012.
(26) Finikova, O. S.; Lebedev, A. Y.; Aprelev, A.; Troxler, T.; Gao, F.; Garnacho, C.; Muro, S.; Hochstrasser, R. M.; Vinogradov, S. A. Oxygen microscopy by two-photon-excited phosphorescence. *ChemPhysChem* **2008**, *9*, 1673−1679.
(27) Sakadžić, S.; Roussakis, E.; Yaseen, M. A.; Mandeville, E. T.; Srinivasan, V. J.; Arai, K.; Ruvinskaya, S.; Devor, A.; Lo, E. H.; Vinogradov, S. A.; et al. Two-photon high-resolution measurement of partial pressure of oxygen in cerebral vasculature and tissue. *Nat. Methods* **2010**, *7*, 755−759.
(28) Lecoq, J.; Parpaleix, A.; Roussakis, E.; Ducros, M.; Houssen, Y. G.; Vinogradov, S. A.; Charpak, S. Simultaneous two-photon imaging of oxygen and blood flow in deep cerebral vessels. *Nat. Med.* **2011**, *17*, 893−898.
(29) Devor, A.; Sakadzic, S.; Saisan, P. A.; Yaseen, M. A.; Roussakis, E.; Srinivasan, V. J.; Vinogradov, S. A.; Rosen, B. R.; Buxton, R. B.; Dale, A. M.; et al. "Overshoot" of O_2 is required to maintain baseline tissue oxygenation at locations distal to blood vessels. *J. Neurosci.* **2011**, *31*, 13676−13681.
(30) Parpaleix, A.; Houssen, Y. G.; Charpak, S. Imaging local neuronal activity by monitoring pO_2 transients in capillaries. *Nat. Med.* **2013**, *19*, 241−246.
(31) Sakadžić, S.; Mandeville, E. T.; Gagnon, L.; Musacchia, J. J.; Yaseen, M. A.; Yucel, M. A.; Lefebvre, J.; Lesage, F.; Dale, A. M.; Eikermann-Haerter, K.; et al. Large arteriolar component of oxygen delivery implies a safe margin of oxygen supply to cerebral tissue. *Nat. Commun.* **2014**, *5*, No. 5734.
(32) Spencer, J. A.; Ferraro, F.; Roussakis, E.; Klein, A.; Wu, J. W.; Runnels, J. M.; Zaher, W.; Mortensen, L. J.; Alt, C.; Turcotte, R.; et al. Direct measurement of local oxygen concentration in the bone marrow of live animals. *Nature* **2014**, *508*, 269−273.
(33) Christodoulou, C.; Spencer, J. A.; Yeh, S. C. A.; Turcotte, R.; Kokkaliaris, K. D.; Panero, R.; Ramos, A.; Guo, G. J.; Seyedhassantehrani, N.; Esipova, T. V.; et al. Live-animal imaging of native haematopoietic stem and progenitor cells. *Nature* **2020**, *578*, 278−283.
(34) Rytelewski, M.; Haryutyunan, K.; Nwajei, F.; Shanmugasundaram, M.; Wspanialy, P.; Zal, M. A.; Chen, C. H.; El Khatib, M.; Plunkett, S.; Vinogradov, S. A.; et al. Merger of dynamic two-photon and phosphorescence lifetime microscopy reveals dependence of lymphocyte motility on oxygen in solid and hematological tumors. *J. Immunother. Cancer* **2019**, *7*, No. 78.
(35) Schilling, K.; El Khatib, M.; Plunkett, S.; Xue, J. J.; Xia, Y. N.; Vinogradov, S. A.; Brown, E.; Zhang, X. P. Electrospun fiber mesh for high-resolution measurements of oxygen tension in cranial bone defect repair. *ACS Appl. Mater. Interfaces* **2019**, *11*, 33548−33558.
(36) Sencan, I.; Esipova, T. V.; Yaseen, M. A.; Fu, B.; Boas, D. A.; Vinogradov, S. A.; Shahidi, M.; Sakadzic, S. Two-photon phosphorescence lifetime microscopy of retinal capillary plexus oxygenation in mice. *J. Biomed. Opt.* **2019**, *23*, No. 126501.
(37) Esipova, T. V.; Barrett, M. J. P.; Erlebach, E.; Masunov, A. E.; Weber, B.; Vinogradov, S. A. Oxyphor 2P: a high-performance probe for deep-tissue longitudinal oxygen imaging. *Cell Metab.* **2019**, *29*, 736−744.
(38) Srivatsan, A.; Missert, J. R.; Upadhyay, S. K.; Pandey, R. K. Porphyrin-based photosensitizers and the corresponding multifunc-

https://dx.doi.org/10.1021/acs.jpca.0c08334
J. Phys. Chem. A 2020, 124, 11038−11050

tional nanoplatforms for cancer-imaging and phototherapy. *J. Porphyrins Phthalocyanines* **2015**, *19*, 109−134.
(39) Abrahamse, H.; Hamblin, M. R. New photosensitizers for photodynamic therapy. *Biochem. J.* **2016**, *473*, 347−364.
(40) Rebane, A. K.; Mikhaylov, A. In *Improved Reference Standards for Femtosecond Three-Photon Excitation of Fluorescence in the Wavelength Range 950−1750 nm*, Multiphoton Microscopy in the Biomedical Sciences XVIII, 2018.
(41) Deng, X.; Zhuang, Z.; Liu, H.; Qiu, P.; Wang, K. Measurement of 3-photon excitation and emission spectra and verification of Kasha's rule for selected fluorescent proteins excited at the 1700-nm window. *Opt. Express* **2019**, *27*, 12723−12731.
(42) Lin, T. C.; Zheng, Q.; Chen, C. Y.; He, G. S.; Huang, W. J.; Ryasnyanskiy, A. I.; Prasad, P. N. Novel fluorophore based on a multi-substituted olefin skeleton with enhanced three-photon absorption in the femtosecond regime. *Chem. Commun.* **2008**, 389−391.
(43) Drobizhev, M.; Rebane, A.; Suo, Z.; Spangler, C. W. One-, two- and three-photon spectroscopy of π-conjugated dendrimers: cooperative enhancement and coherent domains. *J. Lumin.* **2005**, *111*, 291−305.
(44) Simpson, P. V.; Watson, L. A.; Barlow, A.; Wang, G.; Cifuentes, M. P.; Humphrey, M. G. Record multiphoton absorption cross-sections by dendrimer organometalation. *Angew. Chem., Int. Ed.* **2016**, *55*, 2387−2391.
(45) Schwich, T.; Barlow, A.; Cifuentes, M. P.; Szeremeta, J.; Samoc, M.; Humphrey, M. G. Stellar multi-photon absorption materials: Beyond the telecommunication wavelength band. *Chem. − Eur. J.* **2017**, *23*, 8395−8399.
(46) He, G. S.; Tan, L.; Zheng, Q.; Prasad, P. N. Multiphoton-absorbing materials: molecular designs, characterizations and applications. *Chem. Rev.* **2008**, *108*, 1245−1330.
(47) Morisue, M.; Ogawa, K.; Kamada, K.; Ohta, K.; Kobuke, Y. Strong two-photon and three-photon absorptions in the antiparallel dimer of a porphyrin-phthalocyanine tandem. *Chem. Commun.* **2010**, *46*, 2121−2123.
(48) Cohanoschi, I.; Echeverría, L.; Hernández, F. E. Three-photon absorption measurements in hematoporphyrin IX: "Ground-breaking opportunities in deep photodynamic therapy". *Chem. Phys. Lett.* **2006**, *419*, 33−36.
(49) Gouterman, M. Spectra of porphyrins. *J. Mol. Spectrosc.* **1961**, *6*, 138−163.
(50) Finikova, O. S.; Troxler, T.; Senes, A.; DeGrado, W. F.; Hochstrasser, R. M.; Vinogradov, S. A. Energy and electron transfer in enhanced two-photon-absorbing systems with triplet cores. *J. Phys. Chem. A* **2007**, *111*, 6977−6990.
(51) Esipova, T. V.; Rivera-Jacquez, H. J.; Weber, B.; Masunov, A. E.; Vinogradov, S. A. Two-photon absorbing phosphorescent metalloporphyrins: effects of π-extension and peripheral substitution. *J. Am. Chem. Soc.* **2016**, *138*, 15648−15662.
(52) Esipova, T. V.; Rivera-Jacquez, H. J.; Weber, B.; Masunov, A. E.; Vinogradov, S. A. Stabilizing *g*-states in centrosymmetric tetrapyrroles: two-photon-absorbing porphyrins with bright phosphorescence. *J. Phys. Chem. A* **2017**, *121*, 6243−6255.
(53) Mikhailov, I. A.; Tafur, S.; Masunov, A. E. Double excitations and state-to-state transition dipoles in π-π* excited singlet states of linear polyenes: Time-dependent density-functional theory versus multiconfigurational methods. *Phys. Rev. A* **2008**, *77*, No. 012510.
(54) Mikhailov, I. A.; Bondar, M. V.; Belfield, K. D.; Masunov, A. E. Electronic properties of a new two-photon absorbing fluorene derivative: The role of Hartree-Fock exchange in the density functional theory design of improved nonlinear chromophores. *J. Phys. Chem. C* **2009**, *113*, 20719−20724.
(55) Masunov, A. E.; Mikhailov, I. A. Theory and computations of two-photon absorbing photochromic chromophores. *Eur. J. Chem.* **2010**, *1*, 142−161.
(56) Nayyar, I. H.; Masunov, A. E.; Tretiak, S. Comparison of TD-DFT methods for the calculation of two-photon absorption spectra of oligophenylvinylenes. *J. Phys. Chem. C* **2013**, *117*, 18170−18189.
(57) Makarov, N. S.; Drobizhev, M.; Rebane, A. Two-photon absorption standards in the 550-1600 nm excitation wavelength range. *Opt. Express* **2008**, *16*, 4029−4047.
(58) Frisch, M. J.; Trucks, G. W.; Schlegel, H. B.; Scuseria, G. E.; Robb, M. A.; Cheeseman, J. R.; Scalmani, G.; Barone, V.; Mennucci, B.; Petersson, G. A. et al. *Gaussian 09*, revision D.01; Gaussian Inc., 2009.
(59) Andrae, D.; Haussermann, U.; Dolg, M.; Stoll, H.; Preuss, H. Energy-adjusted ab initio pseudopotentials for the 2nd and 3rd row transition elements. *Theor. Chim. Acta* **1990**, *77*, 123−141.
(60) Dunning, T. H., Jr.; Hay, P. J. Gaussian Basis Sets for Molecular Calculations. In *Methods of Electronic Structure Theory*; Schaefer, H. F., III, Ed.; Springer: New York, 1977; Vol. 3, pp 1−27.
(61) Masunov, A. M.; Tretiak, S. Prediction of two-photon absorption properties for organic chromophores using time-dependent density-functional theory. *J. Phys. Chem. B* **2004**, *108*, 899−907.
(62) Marenich, A. V.; Cramer, C. J.; Truhlar, D. G. Universal solvation model based on solute electron density and on a continuum model of the solvent defined by the bulk dielectric constant and atomic surface tensions. *J. Phys. Chem. B* **2009**, *113*, 6378−6396.
(63) Peticolas, W. L. Multiphoton spectroscopy. *Annu. Rev. Phys. Chem.* **1967**, *18*, 233−260.
(64) McClain, W. M. Polarization dependence of three-photon phenomena for randomly oriented molecules. *J. Chem. Phys.* **1972**, *57*, 2264−2272.
(65) Friedrich, D. M. Tensor patterns and polarization ratios for three-photon transitions in fluid media. *J. Chem. Phys.* **1981**, *75*, 3258−3268.
(66) Andrews, D. L.; Ghoul, W. A. Polarization studies in multiphoton absorption spectroscopy. *J. Chem. Phys.* **1981**, *75*, 530−538.
(67) Jagatap, B. N.; Meath, W. J. Contributions of permanent dipole moments to molecular multiphoton excitation cross sections. *J. Opt. Soc. Am. B* **2002**, *19*, 2673−2681.
(68) Cronstrand, P.; Luo, Y.; Ågren, H. Multi-Photon Absorption of Molecules. *Response Theory and Molecular Properties (A Tribute to Jan Linderberg and Poul Jørgensen)*; Elsevier Inc., 2005; pp 1−21.
(69) Cronstrand, P.; Norman, P.; Luo, Y.; Agren, H. Few-states models for three-photon absorption. *J. Chem. Phys.* **2004**, *121*, 2020−2029.
(70) Zhu, L.; Yi, Y.; Shuai, Z.; Schmidt, K.; Zojer, E. Structure to property relationships for multiphoton absorption in covalently linked porphyrin dimers: A correction vector INDO/MRDCI study. *J. Phys. Chem. A* **2007**, *111*, 8509−8518.
(71) Zhu, L.; Yi, Y.; Shuai, Z.; Bredas, J. L.; Beljonne, D.; Zojer, E. Structure-property relationships for three-photon absorption in stilbene-based dipolar and quadrupolar chromophores. *J. Chem. Phys.* **2006**, *125*, No. 044101.
(72) Yi, Y.; Zhu, L.; Shuai, Z. Theoretical designs of molecular photonics materials. *Macromol. Theory Simul.* **2008**, *17*, 12−22.
(73) Meath, W. J.; Jagatap, B. N. On the effects of permanent molecular dipoles in the simultaneous absorption of two photons: Full generalized rotating wave approximation versus analytical results. *J. Chem. Phys.* **2013**, *139*, No. 144104.
(74) Friese, D. H.; Beerepoot, M. T.; Ringholm, M.; Ruud, K. Open-ended recursive approach for the calculation of multiphoton absorption matrix elements. *J. Chem. Theory. Comput.* **2015**, *11*, 1129−1144.
(75) Boyd, R. W. *Non-linear Optics*; Elsevier Inc.: Oxford, U.K., 2008.
(76) Mandal, A. K.; Taniguchi, M.; Diers, J. R.; Niedzwiedzki, D. M.; Kirmaier, C.; Lindsey, J. S.; Bocian, D. F.; Holten, D. Photophysical properties and electronic structure of porphyrins bearing zero to four *meso*-phenyl substituents: new insights into seemingly well understood tetrapyrroles. *J. Phys. Chem. A* **2016**, *120*, 9719−9731.
(77) Esipova, T. V.; Vinogradov, S. A. Synthesis of phosphorescent asymmetrically π-extended porphyrins for two-photon applications. *J. Org. Chem.* **2014**, *79*, 8812−8825.

https://dx.doi.org/10.1021/acs.jpca.0c08334
J. Phys. Chem. A 2020, 124, 11038−11050

(78) Bajema, L.; Gouterman, M.; Rose, C. Porphyrins XXIII: Fluorescene of the second excited singlet and quasiline structure of Zinc Tetrabenzoporphyrin. *J. Mol. Spectrosc.* **1971**, *39*, 421−431.
(79) Edwards, L.; Gouterman, M.; Rose, C. B. Synthesis and vapor spectra of Zinc tetrabenzoporphyrin. *J. Am. Chem. Soc.* **1976**, *98*, 7638−7641.
(80) Rosa, A.; Ricciardi, G.; Baerends, E. J.; van Gisbergen, S. J. A. The optical spectra of NiP, NiPz, NiTBP, and NiPc: Electronic effects of meso-tetraaza substitution and tetrabenzo annulation. *J. Phys. Chem. A* **2001**, *105*, 3311−3327.
(81) Rogers, J. E.; Nguyen, K. A.; Hufnagle, D. C.; McLean, D. G.; Su, W. J.; Gossett, K. M.; Burke, A. R.; Vinogradov, S. A.; Pachter, R.; Fleitz, P. A. Observation and interpretation of annulated porphyrins: studies on the photophysical properties of *meso*-tetraphenylmetalloporphyrins. *J. Phys. Chem. A* **2003**, *107*, 11331−11339.
(82) Eastwood, D.; Gouterman, M. Porphyrins. XVIII. Luminescence of (Co), (Ni), Pd, Pt complexes. *J. Mol. Spectrosc.* **1970**, *35*, 359−375.
(83) Kim, D. H.; Holten, D.; Gouterman, M.; Buchler, J. W. Comparative photophysics of platinum(II) and platinum(IV) porphyrins. *J. Am. Chem. Soc.* **1984**, *106*, 4015−4017.
(84) Lebedev, A. Y.; Filatov, M. A.; Cheprakov, A. V.; Vinogradov, S. A. Effects of structural deformations on optical properties of tetrabenzoporphyrins: free-bases and Pd complexes. *J. Phys. Chem. A* **2008**, *112*, 7723−7733.
(85) Brouwer, A. M. Standards for photoluminescence quantum yield measurements in solution (IUPAC Technical Report). *Pure Appl. Chem.* **2011**, *83*, 2213−2228.
(86) Kajzar, F.; Messier, J. 3rd harmonic generation in liquids. *Phys. Rev. A* **1985**, *32*, 2352−2363.
(87) Tsang, T. Y. F. Optical 3rd harmonic generation at interfaces. *Phys. Rev. A* **1995**, *52*, 4116−4125.
(88) Squier, J. A.; Muller, M.; Brakenhoff, G. J.; Wilson, K. R. Third harmonic generation microscopy. *Opt. Express* **1998**, *3*, 315−324.
(89) Barad, Y.; Eisenberg, H.; Horowitz, M.; Silberberg, Y. Nonlinear scanning laser microscopy by third harmonic generation. *Appl. Phys. Lett.* **1997**, *70*, 922−924.
(90) Yelin, D.; Silberberg, Y. Laser scanning third-harmonic-generation microscopy in biology. *Opt. Express* **1999**, *5*, 169−175.
(91) Clay, G. O.; Millard, A. C.; Schaffer, C. B.; Aus-Der-Au, J.; Tsai, P. S.; Squier, J. A.; Kleinfeld, D. Spectroscopy of third-harmonic generation: evidence for resonances in model compounds and ligated hemoglobin. *J. Opt. Soc. Am. B* **2006**, *23*, 932−950.
(92) Pawlicki, M.; Collins, H. A.; Denning, R. G.; Anderson, H. L. Two-photon absorption and the design of two-photon dyes. *Angew. Chem., Int. Ed.* **2009**, *48*, 3244−3266.

https://dx.doi.org/10.1021/acs.jpca.0c08334
J. Phys. Chem. A 2020, 124, 11038−11050